SSD-TR-92-12

AEROSPACE REPORT NO.
TR-0089(4925-05)-1

Dielectric Ribbon Waveguide--An Optimum Configuration for Ultralow-Loss Millimeter/Submillimeter Dielectric Waveguide

Prepared by

C. YEH AND J. CHU
University of Los Angeles, California

and

F. I. SHIMABUKURO
Electronics Research Laboratory
Laboratory Operations
The Aerospace Corporation

14 April 1991

Prepared for

SPACE SYSTEMS DIVISION
AIR FORCE SYSTEMS COMMAND
Los Angeles Air Force Base
P. O. Box 92960
Los Angeles, CA 90009-2960

Engineering and Technology Group

THE AEROSPACE CORPORATION
El Segundo, California

This report was submitted by The Aerospace Corporation, El Segundo, CA 90245-4691, under Contract No. F04701-88-C-0089 with the Space Systems Division. P. O. Box 92960, Los Angeles, CA 90009-2960. It was reviewed and approved for The Aerospace Corporation by M. J. Daugherty, Director, Electronics Research Laboratory. Capt George Besenyei was the project officer for the Mission-Oriented Investigation and Experimentation (MOIE) program.

This report has been reviewed by the Public Affairs Office (PAS) and is releasable to the National Technical Information Service (NTIS). At NTIS, it will be available to the general public, including foreign nationals.

This technical report has been reviewed and is approved for publication. Publication of this report does not constitute Air Force approval of the report's findings or conclusions. It is published only for the exchange and stimulation of ideas.

MARTIN K. WILLIAMS, Capt, USAF
Mgr, Space Systems Integration
DCS for Program Management

GEORGE M. BESENYEI, Capt, USAF
Chief, Engineering and Test
SATCOM Program Office

UNCLASSIFIED

SECURITY CLASSIFICATION OF THIS PAGE

REPORT DOCUMENTATION PAGE

1a. REPORT SECURITY CLASSIFICATION Unclassified	1b. RESTRICTIVE MARKINGS
2a. SECURITY CLASSIFICATION AUTHORITY	3. DISTRIBUTION/AVAILABILITY OF REPORT Approved for public release; distribution unlimited
2b. DECLASSIFICATION/DOWNGRADING SCHEDULE	
4. PERFORMING ORGANIZATION REPORT NUMBER(S) TR-0089(4925-05)-1	5. MONITORING ORGANIZATION REPORT NUMBER(S) SSD-TR-92-12
6a. NAME OF PERFORMING ORGANIZATION The Aerospace Corporation Laboratory Operations 6b. OFFICE SYMBOL *(If applicable)*	7a. NAME OF MONITORING ORGANIZATION Space Systems Division
6c. ADDRESS *(City, State, and ZIP Code)* El Segundo, CA 90245-4691	7b. ADDRESS *(City, State, and ZIP Code)* Los Angeles Air Force Base Los Angeles, CA 90009-2960
8a. NAME OF FUNDING/SPONSORING ORGANIZATION 8b. OFFICE SYMBOL *(If applicable)*	9. PROCUREMENT INSTRUMENT IDENTIFICATION NUMBER F04701-88-C-0089
8c. ADDRESS *(City, State, and ZIP Code)*	10. SOURCE OF FUNDING NUMBERS PROGRAM ELEMENT NO. / PROJECT NO. / TASK NO. / WORK UNIT ACCESSION NO.

11. TITLE *(Include Security Classification)*
Dielectric Ribbon Waveguide--An Optimum Configuration for Ultralow-Loss Millimeter/Submillimeter Dielectric Waveguide

12. PERSONAL AUTHOR(S) Yeh, C., and Chu, J. (University of Los Angeles, California); and Shimabukuro, F. I. (The Aerospace Corporation)

13a. TYPE OF REPORT	13b. TIME COVERED FROM _____ TO _____	14. DATE OF REPORT *(Year, Month, Day)*	15. PAGE COUNT
		14 April 1991	44

16. SUPPLEMENTARY NOTATION

17. COSATI CODES			18. SUBJECT TERMS *(Continue on reverse if necessary and identify by block number)*
FIELD	GROUP	SUB-GROUP	Dielectric Ribbon Waveguide Low-Loss Dielectric Waveguide Millimeter Waveguide

19. ABSTRACT *(Continue on reverse if necessary and identify by block number)*

Dielectric ribbon waveguide supporting the eHE11 dominant mode can be made to yield an attenuation constant for this mode that is less than 20 dB/km in the millimeter/submillimeter wavelength range. The waveguide is made with a high-dielectric-constant, low-loss material such as alumina or sapphire. The waveguide takes the form of thin dielectric ribbon surrounded by lossless dry air. Detailed theoretical analysis of the attenuation and field extent characteristics for the low-loss dominant eHE11 mode along a ribbon dielectric waveguide was performed using the exact finite-element technique as well as two approximate techniques. Analytical predictions were then verified by measurements on ribbon guides made with rexolite, using the highly sensitive cavity resonator method. Excellent agreement was found.

20. DISTRIBUTION/AVAILABILITY OF ABSTRACT	21. ABSTRACT SECURITY CLASSIFICATION
[X] UNCLASSIFIED/UNLIMITED [ ] SAME AS RPT. [ ] DTIC USERS	Unclassified

22a. NAME OF RESPONSIBLE INDIVIDUAL	22b. TELEPHONE *(Include Area Code)*	22c. OFFICE SYMBOL

PREFACE

The authors express their gratitude to H. B. Dyson for being primarily responsible for obtaining the measurement data. They also would like to thank S. L. Johns for assisting in the measurements and plotting some of the data, and G. G. Berry for fabricating the dielectric waveguides. The authors at UCLA wish to thank Dr. J. Hamada and Dr. B. Wong for their enthusiastic support of the UCLA-TRW MICRO Program.

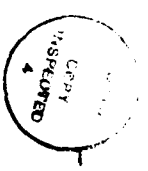

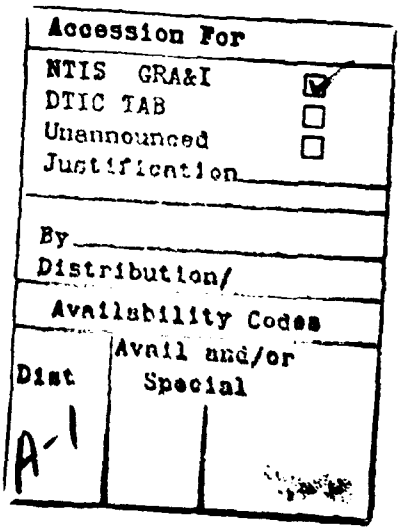

CONTENTS

FIGURES

FIGURES (Continued)

TABLES

I. INTRODUCTION

The phenomenal success of the dielectric fiber as an ultralow-loss optical waveguide has enticed us to reconsider the viability of the dielectric rod as a low-loss millimeter/submillimeter (mm/sub-mm) waveguide. A survey of commercially available materials shows that two classes of material may be excellent candidates as low-loss dielectric materials for mm/sub-mm wave applications:[1-4] (1) Crystalline material such as quartz, alumina, and sapphire; and (2) Nonpolar polymers such as poly-4-methylpentene-1 (TPX), Teflon (PTFE), polyethylene (LDPE), and polypropylene. Another way to minimize the attenuation constant for the guided wave along a dielectric structure is to use special waveguide configurations. This report will first survey commercially available low-loss dielectric material and highlight possible ways to reduce the loss factor. Then the report will identify low-loss configurations. We will show that a properly configured waveguide can support the dominant mode with a loss factor as much as 50 to 100 times below that for an equivalent circular dielectric waveguide. A loss factor of less than 20 dB/km can be realized with presently available material. This waveguide takes the form of a thin dielectric ribbon surrounded by lossless dry air. Theoretical analyses have been performed based on three approaches: the slab approach,[5] Marcatili's approach,[6] and the exact finite-element approach.[7] Experimental verification of selected cases has also been carried out using the unique ultrahigh-Q, dielectric-waveguide, cavity-resonator apparatus that we developed.[8] Our investigation shows that it is feasible to design a long-distance mm/sub-mm wave communication line with losses approaching 20 dB/km using the dielectric ribbon waveguide made with commercially available low-loss, high-dielectric-constant material.

II. LOW-LOSS DIELECTRIC MATERIAL

A series of very detailed measurements in the mm/sub-mm wavelength range on the dielectric constant and loss tangent of groups of promising low-loss material has been performed by the MIT 'Mag-Lab' group in recent years. Results of its findings were summarized in a comprehensive paper by Afsar and Button.[1] Afsar[2] also presented his measured results on several very low-loss nonpolar polymers. Two types of commercially available low-loss material are listed in Table 1. This list reveals that the polymer material, in general, has a much lower dielectric constant than the crystalline material. The smallest loss tangent is of the order of 10^{-4}. If we use a nominal dielectric constant of 2.0, the attenuation constant for plane wave in this bulk material is 1.3 dB/m at 100 GHz, which is already less than the 2.4 dB/m loss for conventional metallic waveguides at this frequency. The attenuation constant for plane wave is calculated from the following equation:[9]

$$\alpha = 8.686(\pi\sqrt{\varepsilon_1}/\lambda_0) \tan \delta \ (\text{dB/m}) \qquad (1)$$

where ε_1 is the relative dielectric constant, λ_0 is the free-space wavelength, and tan δ is the loss tangent. According to Eq. (1), it appears that, in addition to requiring as small a loss tangent as possible, a lower dielectric constant is also helpful in achieving lower loss. Hence, flexible nonpolar polymers such as LDPE and PTFE may be good choices for making low-loss mm/sub-mm waveguides. However, this conclusion can be deceiving because it is based purely on the low-loss property of the waveguide material, i.e., only bulk material loss is considered, and the effect of waveguide configuration on losses has not been included. If the configuration effect is taken into account, material with lower dielectric constant may not offer the advantage of lower attenuation constant as indicated by Eq. (1). (Detailed consideration of the configuration factor will be given in Section III.)

Table 1. Crystalline and Polymer Materials

Crystalline Material[3,4]	Dielectric Constant	Loss Tangent
ZnS (at 100 GHz)	8.4	2×10^{-3}
Alumina (at 10 GHz)	9.7	2×10^{-4}
Sapphire (at 100 GHz)	9.3-11.7	4×10^{-4}
Quartz (at 100 GHz)	3.8-4.8	5×10^{-4}
KRS-5 (at 94.75 GHz)	30.5	1.9×10^{-2}
KRS-6 (at 94.75 GHz)	28.5	2.3×10^{-2}
$LiNbO_3$ (at 94.75 GHz)	6.7	8×10^{-3}

Polymer Material[1,2]	Dielectric Constant	Loss Tangent
Teflon (at 100 GHz) (PTFE)	2.07	2×10^{-4}
Rexolite (at 10 GHz)	2.55	1×10^{-3}
RT-duroid 5880 (at 10 GHz)	2.2	9×10^{-4}
Polyethylene (at 100 GHz) (LDPE)	2.306	3×10^{-4}
Poly-4 methylpentene-1 (TPX) (at 100 GHz)	2.071	6×10^{-4}
Polypropylene (at 100 GHz)	2.261	7×10^{-4}

One approach for constructing low-loss waveguide material is to use an artificial dielectric.[10,11] The artificial dielectric may be composed of alternate longitudinal layers of low-loss, high-dielectric-constant material such as quartz and air. This approach may be interpreted as a way of altering the configuration of guided-wave structure, which will be addressed in the next section. The artificial dielectric material may also be constructed with small particles (size $<< \lambda_0$) of low-loss, high-dielectric-constant material such as small quartz or sapphire spheres, suspended in air. For example, the dielectric constant and loss tangent of sapphire at 100 GHz is 10 and 4×10^{-4}, respectively. Roughly speaking, if a volume contains 10% of sapphire powder (small spheres), the equivalent dielectric constant would be approximately 2, and the equivalent loss tangent could be reduced to 4×10^{-5}. So a high-dielectric-constant, low-loss crystalline material is an excellent candidate for the construction of artificial low-loss dielectric materials.

Returning to our discussion of polymers, we know that the molecules that make up a typical molecular crystal are bound together by strong valence forces and are held in their correct places in the lattice by much weaker van der Waals forces. The major absorption mechanisms in nonpolar polymers in the mm/sub-mm region are[2]

1. Resonances of normal modes of macromolecular helices.
2. Absorption spectrum of impurities such as catalyst residues, antioxidants, ionic impurities, plasticizers, catalyst residues, and other additives.
3. Amorphous behavior of polymers.

Recognizing the mechanisms that are generally responsible for the absorption spectra of these polymers in the mm/sub-mm/far infrared region, one may selectively improve the loss characteristics of a given polymer. For example, impurities may be controlled and reduced; other ions may be introduced to stiffen the long chain molecules so that the chain-twisting vibrations in the mm wave frequencies may be dampened, reducing the absorptions at these frequencies; and the amorphous characteristics of the polymer can be altered by using different cooling/melting processes.

In the following section, it will be shown that a high-dielectric-constant material with low-loss tangent is the material of choice for the construction of specially configured ultralow-loss waveguides.

III. LOW-LOSS CONFIGURATION STUDY

Reducing the loss tangent of the bulk material will certainly improve the attenuation constant of a guided wave along a dielectric waveguide made with such material. The size and shape of the waveguide can also influence the attenuation. The attenuation constant for a dielectric waveguide with arbitrary cross-sectional shape is given by the following expression:[9]

$$\alpha = 8.686\ \pi(1/\lambda_0)(L_1 + L_0),\ (\mathrm{dB/m}) \tag{2}$$

where

$$L_{1,0} = (\varepsilon_{1,0})\ \tan\ \delta_{1,0} R_{1,0} \tag{3}$$

$$R_{1,0} = \left| \frac{\int_{A_{1,0}} (\underline{E}_{1,0} \cdot \underline{E}^*_{1,0}) dA}{\sqrt{\frac{\mu}{\varepsilon}}\left[\int_{A_1} \underline{e}_z \cdot (\underline{E}_1 \times \underline{H}^*_1) dA + \int_{A_0} \underline{e}_z \cdot (\underline{E}_0 \times \underline{H}^*_0) dA\right]} \right| \tag{4}$$

The subscripts 1 and 0 refer, respectively, to the core region and the cladding region of the guide; $\varepsilon_{1,0}$ and tan $\delta_{1,0}$ are, respectively, the relative dielectric constant and loss tangent of the dielectric material; λ_0 is the free-space wavelength; ε_0 and μ are, respectively, the permittivity and permeability of free space; $\underline{e}_z$ is the unit vector in the direction of propagation; A_1 and A_0 are, respectively, the cross-sectional areas of the core and the cladding region; and $\underline{E}$ and $\underline{H}$ are the electric and magnetic field vectors of the guided mode under consideration.

If the core and cladding regions contain similar dielectric material, as in the case of optical fiber waveguide, the attenuation constant α will be relatively insensitive to the geometry of the guide because $(R_1 + R_0)$ will be

insensitive to the geometry of the waveguide. For this case, the attenuation of the wave is determined totally by the loss tangent of the material, and the guide configuration is unimportant. On the other hand, if the cladding region (region 0) contains low-loss dry air or is empty vacuum, then the loss factor $\epsilon_1 R_1$, which is sensitive to the guide configuration and the frequency of operation, will play an important role in the determination of the attenuation constant of the mode guided by the dielectric structure. This loss factor $\epsilon_1 R_1$ could vary from a very small value to $\sqrt{\epsilon_1}$, which is the loss factor for a plane wave propagating in a dielectric medium with relative dielectric constant ϵ_1. So, for a given operating frequency, the smaller the factor $\epsilon_1 R_1$, the more desirable the configuration. As an example, Fig. 1 reveals the $\epsilon_1 R_1$ factor for an elliptical PTFE dielectric waveguide supporting the dominant ${}_eHE_{11}$ mode as a function of the normalized cross-sectional area for different (major axis)/(minor axis) ratios. As shown, a mere flattening of a circular dielectric rod along the maximum intensity of the electric field lines for the dominant ${}_eHE_{11}$ mode can improve the $\epsilon_1 R_1$ factor (hence, α) by a factor of 2 or more.[9] It appears that flattening the circular dielectric rod tends to redistribute and spread out the electric field intensities so that the factor $\int_{A_1} (\underline{E}_1 \cdot \underline{E}_1^*)\, dA$ in Eq. (4) (hence, α) is substantially reduced. This deduction leads us to conclude that a very flat elliptical cylinder or simply a thin ribbon may be an extremely attractive low-loss configuration.

A. WAVE GUIDANCE ALONG A DIELECTRIC SLAB

Let us now consider the problem of wave guidance by an infinite flat plate, as shown in Fig. 2. Two types of dominant modes may exist on this structure: the transverse magnetic (TM) mode (with E_y, E_z, H_x), which is the low-loss mode; and the transverse electric (TE) mode (with H_y, H_z, E_x), which is the high-loss mode. The field components for these modes are[5,10]

TM Wave

In region 1 (the core region),

$$E_y^{(1)} = \frac{-j\beta}{p_1} B \cos p_1 y$$

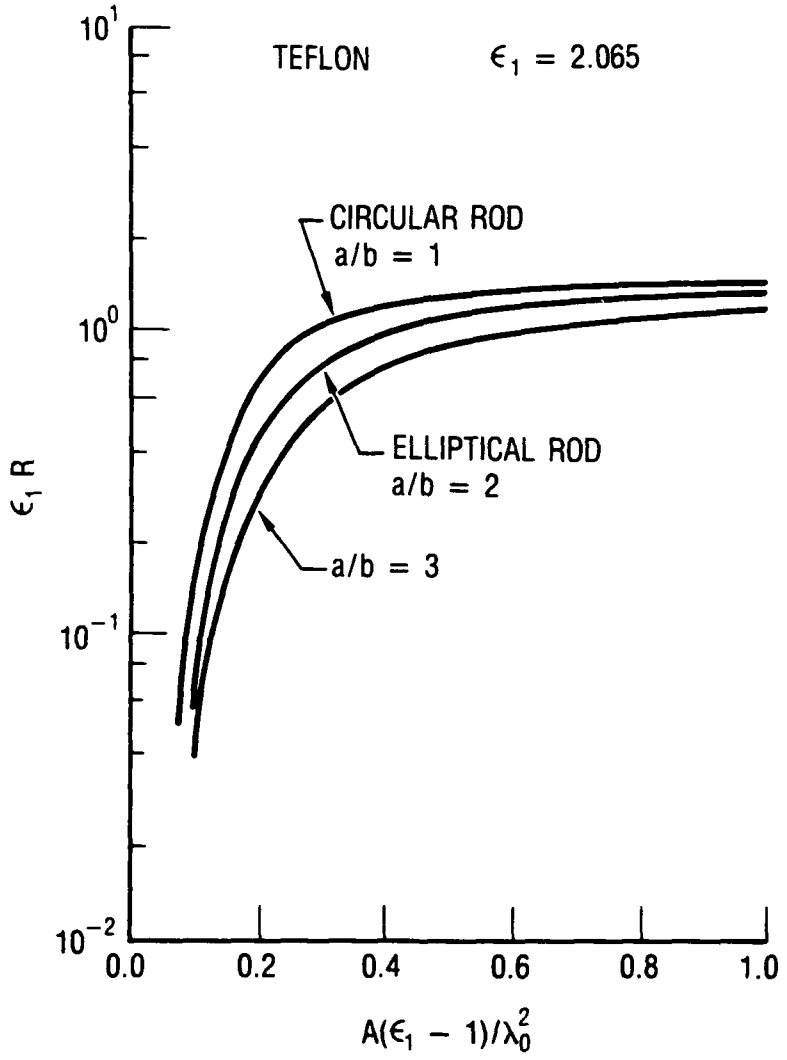

Fig. 1. Configuration Loss Factor $\epsilon_1 R$ as a Function of Normalized Frequency for an Elliptical Teflon Rod Supporting the Dominant $_eHE_{11}$ Mode. A is the cross-sectional area, λ_0 is the free-space wavelength, a is the semi-major axis of the elliptical rod, and b is the semi-minor axis. Note that flatter rod yields smaller configuration loss factor for the same cross-sectional area.

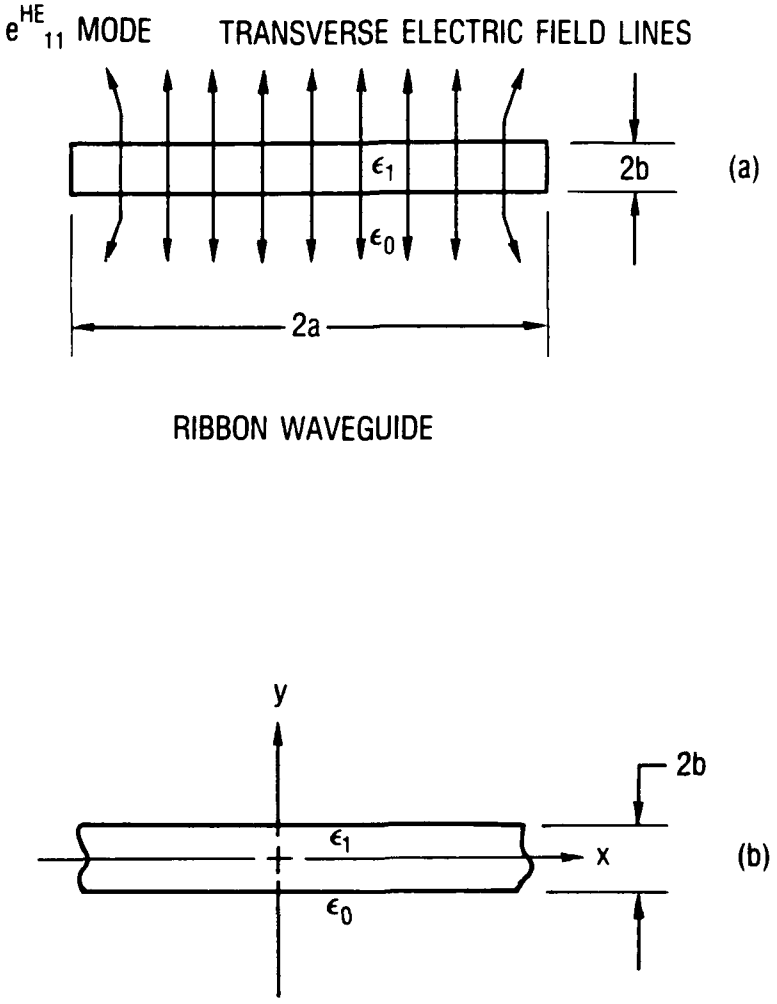

Fig. 2. Cross-sectional Geometries for Ribbon Waveguide and Slab Waveguide

$$E_z^{(1)} = B \sin p_1 y$$

$$H_x^{(1)} = \frac{-j\omega\varepsilon_1\varepsilon}{p_1} B \cos p_1 y \qquad (5)$$

and in region 0 (the cladding region),

$$E_y^{(0)} = \frac{-j\beta}{p_0} C\, e^{-p_0 y}$$

$$E_z^{(0)} = C\, e^{-p_0 y}$$

$$H_x^{(0)} = \frac{-j\omega\varepsilon_0\varepsilon}{p_0} C\, e^{-p_0 y} \qquad (6)$$

with

$$k_0^2 = \omega^2\mu\varepsilon_0\varepsilon,\ k_1^2 = \omega^2\mu\varepsilon_1\varepsilon$$

$$p_0^2 = \beta^2 - k_0^2 \text{ and } p_1^2 = k_1^2 - \beta^2$$

TE Wave

In region 1 (the core region),

$$H_y^{(1)} = \frac{j\beta D}{p_1} \cos p_1 y$$

$$H_z^{(1)} = D \sin p_1 y$$

$$E_x^{(1)} = \frac{j\omega\mu D}{p_1} \cos p_1 y \qquad (7)$$

and in region 0 (the cladding region),

$$H_y^{(0)} = \frac{j\beta}{p_0} F e^{-p_0 y}$$

$$H_z^{(0)} = F e^{-p_0 y}$$

$$E_x^{(0)} = \frac{j\omega\mu}{p_0} F e^{-p_0 y} \qquad (8)$$

We have assumed that the expressions for the field components of all modes are multiplied by the factor $\exp(j\omega t - j\beta z)$, which will be suppressed throughout the equations. In Eqs. (5)-(8), β and ω are, respectively, the propagation constant and angular frequency of the wave, and z is the direction of propagation of the wave. Matching the tangential electric and magnetic fields at the boundary surfaces $y = \pm b$ yields the dispersion relations for the TM and TE modes, from which the $\omega - \beta$ characteristics for these modes may be found. The dispersion relations and the ratios of unknown coefficients are

TM Wave

$$\tan p_1 b = \frac{\varepsilon_1}{\varepsilon_0} \frac{p_0 b}{p_1 b}, \qquad p_1^2 + p_0^2 = k_0^2 \left(\frac{\varepsilon_1}{\varepsilon_0} - 1\right)$$

$$\frac{B}{C} = \frac{e^{-p_0 b}}{\sin p_1 b} \qquad (9)$$

TE Wave

$$\tan p_1 b = \frac{p_0 b}{p_1 b}, \qquad p_1^2 + p_0^2 = k_0^2 \left(\frac{\varepsilon_1}{\varepsilon_0} - 1\right)$$

$$\frac{D}{F} = \frac{e^{-p_0 b}}{\sin p_1 b} \qquad (10)$$

Referring to Eq. (4), one may also calculate the configuration loss factor R as follows:

$$R^{(TM)} = \frac{(p_0 b)^3}{2(p_1 b)(k_0 b)(\beta b)} \frac{\{2p_1 b[1 + (\frac{\beta b}{p_1 b})^2] - [1 - (\frac{\beta b}{p_1 b})^2]\sin 2p_1 b\}}{[\frac{1}{2}(\frac{p_0 b}{p_1 b})^3 \frac{\varepsilon_1}{\varepsilon_0}(2p_1 b + \sin 2p_1 b) + \sin^2 p_1 b]} \quad (11)$$

$$R^{(TE)} = \frac{1}{2}\frac{k_0 b}{\beta b}(\frac{p_0 b}{p_1 b})^3 \frac{(2p_1 b + \sin 2p_1 b)}{[(\frac{p_0 b}{p_1 b})^3 \frac{1}{2}(2p_1 b + \sin 2p_1 b) + \sin^2 p_1 b]} \quad (12)$$

As expected, one can easily show the limiting case for $R^{(TE)}$ and $R^{(TM)}$ as $(2b/\lambda_0) \to \infty$:

$$R^{(TE)} = R^{(TM)} \to 1/\sqrt{\varepsilon_1}$$

Although $R^{(TM)}$ and $R^{(TE)}$ approach the same limit as $2b/\lambda_0$ approaches ∞, the behavior of $R^{(TM)}$ vs $2b/\lambda_0$ and that of $R^{(TE)}$ vs $2b/\lambda_0$ is very different. Figure 3 exhibits plots of $\varepsilon_1 R^{(TM)}$, $\varepsilon_1 R^{(TE)}$ vs $2b/\lambda_0$ for different values of ε_1. The normalized coefficient $R^{(TM),(TE)}\varepsilon_1$ is used because it is proportional to the attenuation constant $\alpha^{(TM),(TE)}$. For a given $2b/\lambda_0$ and ε_1, $\varepsilon_1 R^{(TM)}$, in general, is significantly lower than $\varepsilon_1 R^{TE}$, indicating that the dominant TM mode is the low-loss mode. The ratios of $[\varepsilon_1 R^{(TE)}]/[\varepsilon_1 R^{(TM)}]$ vs $2b/\lambda_0$ for three values of ε_1 are shown in Fig. 4. Note that the ratio is higher for a higher ε_1. For example, at the nominal operating frequency of $2b/\lambda_0 = 0.1$, when $\varepsilon_1 = 2.04$ (PTFE), the ratio $\varepsilon_1 R^{(TE)}/\varepsilon_1 R^{(TM)}$ is 6; when $\varepsilon_1 = 2.55$ (rexolite), the ratio is 10; and when $\varepsilon_1 = 4$ (quartz), the ratio is 19. Thus the loss factor for TM mode is 19 times smaller than the loss factor for TE mode for material with higher dielectric constant. This fact appears to suggest that high-dielectric-constant material with low-loss tangent is the most desirable material for low-loss dielectric waveguides.

The field guided along a dielectric waveguide without cladding material extends into the region beyond the dielectric core. Therefore, it is of interest to learn the relationship between the loss factor $\varepsilon_1 R$ and the field extent beyond the core region. In Fig. 5, the loss factor $\varepsilon_1 R$ is plotted

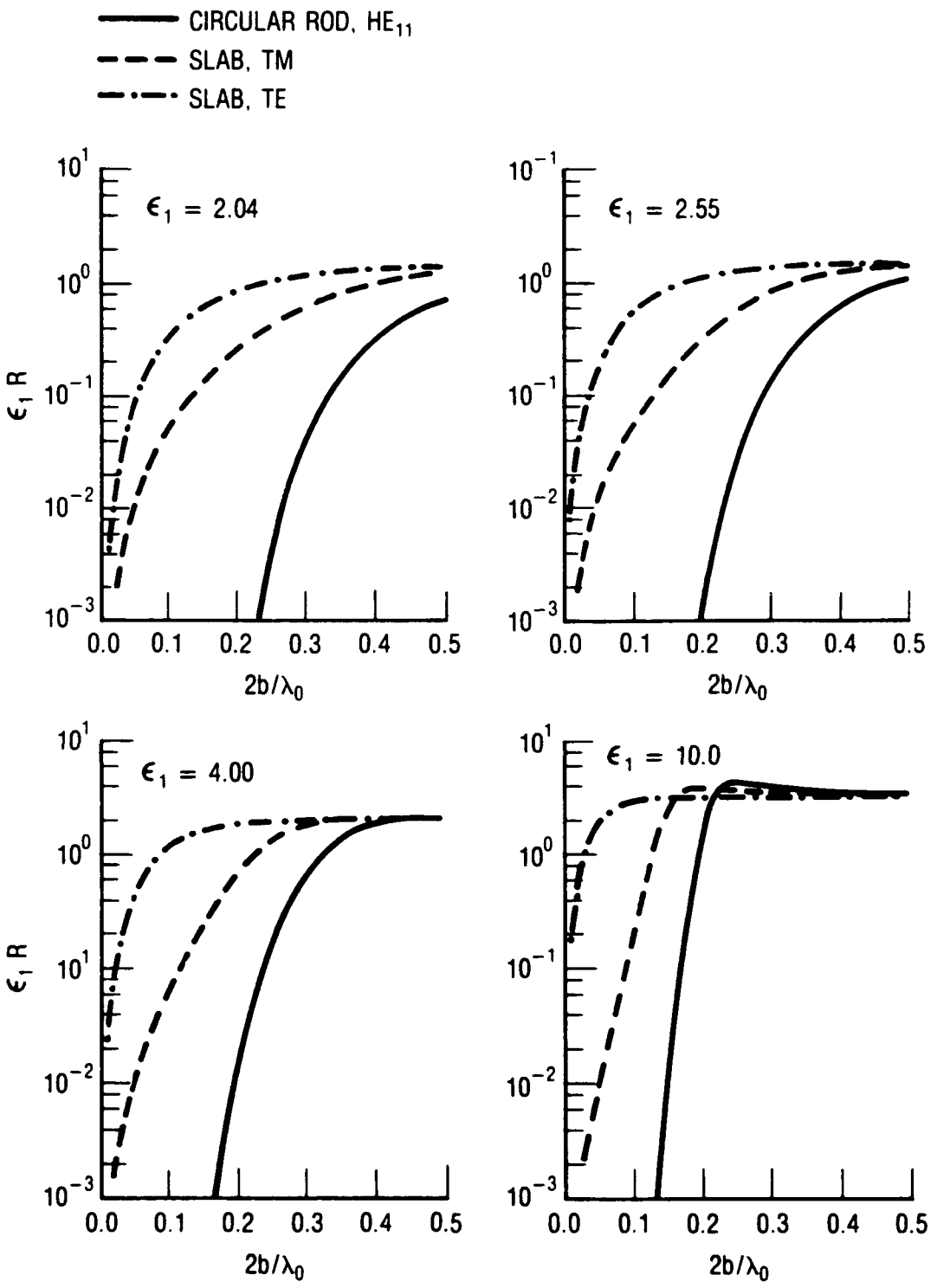

Fig. 3. Configuration Loss Factor $\epsilon_1 R$ as a Function of Normalized Frequency for a Dielectric Slab of Thickness 2b Supporting the Dominant TE and the Dominant TM Modes and for a Circular Rod of Radius b Supporting the Dominant HE_{11} Mode for Various Dielectric Material

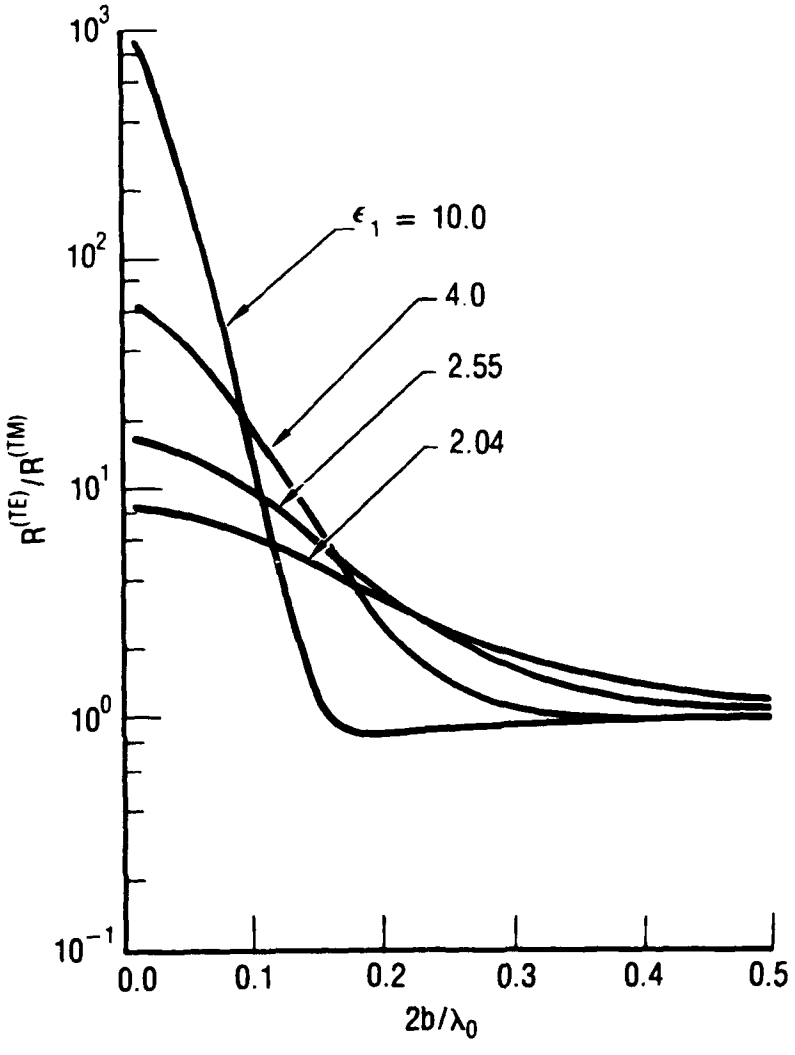

Fig. 4. Ratio of the Configuration Loss Factor for TE and TM vs the Normalized Frequency for Various Dielectric Material. Note that the effect of higher dielectric constant material on the ratio is much more pronounced.

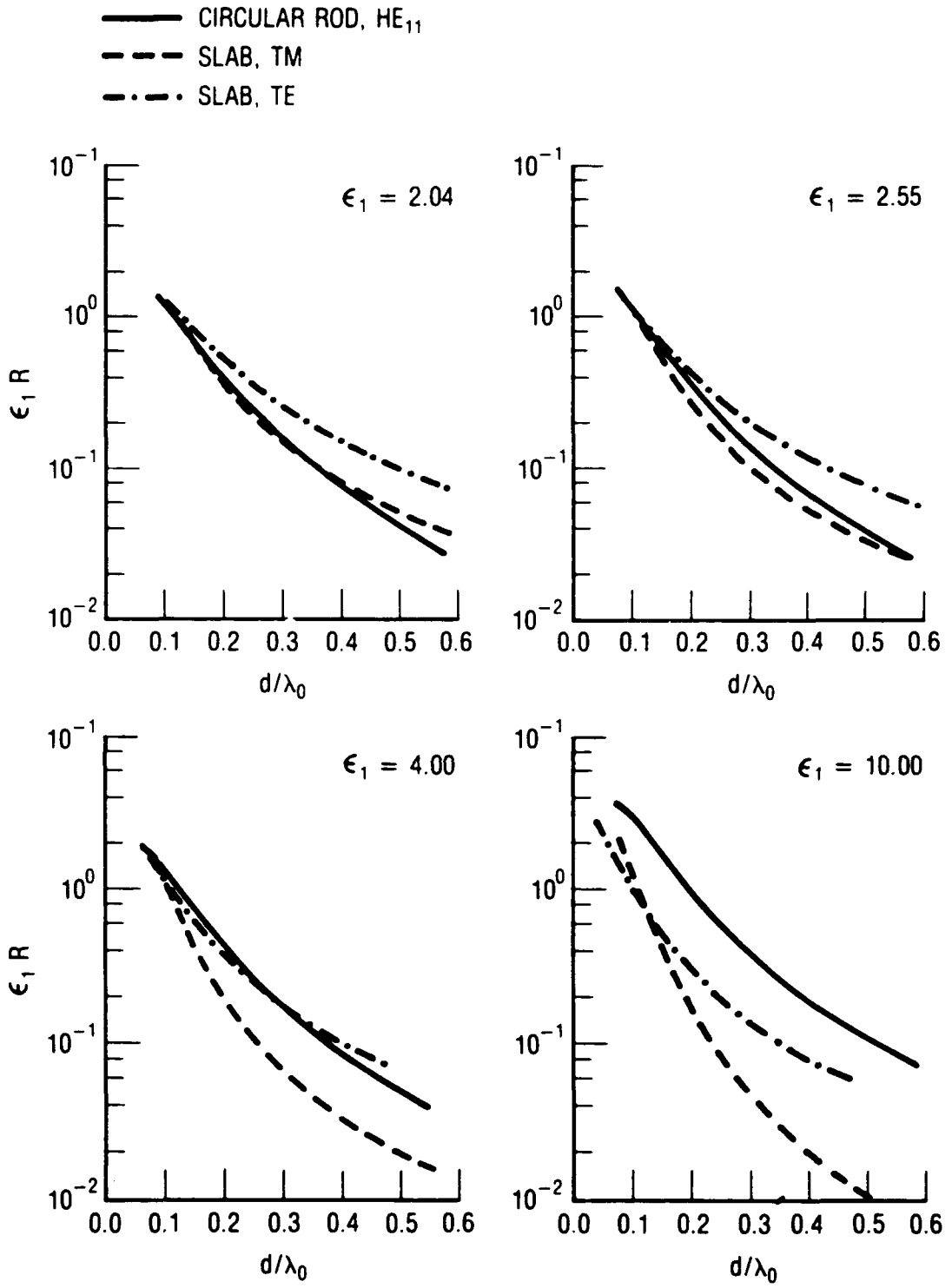

Fig. 5. Configuration Loss Factor $\epsilon_1 R$ as a Function of Normalized Power-Decaying Distance d/λ_0. d is the 1/e power-decaying distance from the surface of the slab or rod, as appropriate. Note that for high dielectric constant material, the power-decaying distance is much shorter for a slab guide than that for a circular rod guide for the same configuration loss factor.

against the normalized field extent beyond the core surface. The field extent is expressed by the distance d from the core surface at which the power density of the guided mode has decayed to 1/e of its value at the core surface, divided by the free space wavelength. So, given $\varepsilon_1 R$ and ε_1, one may obtain the normalized distance from the core surface at which the guided power has decayed to its 1/e value at the core surface. For example, if $\varepsilon_1 R$ is 0.1 and ε_1 = 4.0 (quartz), d/λ_0 = 0.26 for the low-loss TM mode on a slab, d/λ_0 = 0.38 for the HE_{11} mode on a circular rod, and d/λ_0 = 0.41 for the high-loss TE mode on a slab.

B. WAVE GUIDANCE ALONG A DIELECTRIC RIBBON

The dominant ${}_eHE_{11}$ mode guided along a flat dielectric ribbon with aspect ratio greater than, say, 10, must behave similarly to the dominant TM mode guided along a dielectric slab. The only significant differences between the two modes must result from the fringing fields at the edges of the flat ribbon guide. Recognizing these facts, one may use the slab results to obtain the approximate results for the ${}_{e,0}HE_{11}$ modes along a dielectric ribbon guide with high aspect ratio. At very low frequencies, the fields extend further from the waveguide, and the field pattern for an infinite slab would be substantially different from that of a ribbon structure. At these frequencies, the behavior of the loss factor for the infinite slab and ribbon will also be very different. This very low frequency region would not be the region of interest, because the mode is too loosely guided for any practical applications. In Fig. 6, the loss factor $\varepsilon_1 R$ is plotted against the normalized area, $A(\varepsilon_1 - 1)/\lambda_0^2$, where A is the cross-sectional area of the guide. The figure reveals a dramatic difference between the loss factors for the ribbon TM (${}_eHE_{11}$) mode, the ribbon TE (${}_0HE_{11}$) mode, and the circular rod HE_{11} mode for the same normalized area. The loss factor for a flat ribbon guide supporting the ${}_eHE_{11}$ mode could be as much as 100 times smaller than that for a circular rod guide supporting the HE_{11} mode. Furthermore, for a rather broad region of normalized area, the loss factor, $\varepsilon_1 R$, is reasonably flat for the ribbon guide, while it is rather steep for a circular rod guide, indicating that the ribbon guide possesses rather stable low-loss behavior for any possible fluctuation in operating frequencies or cross-sectional area changes.

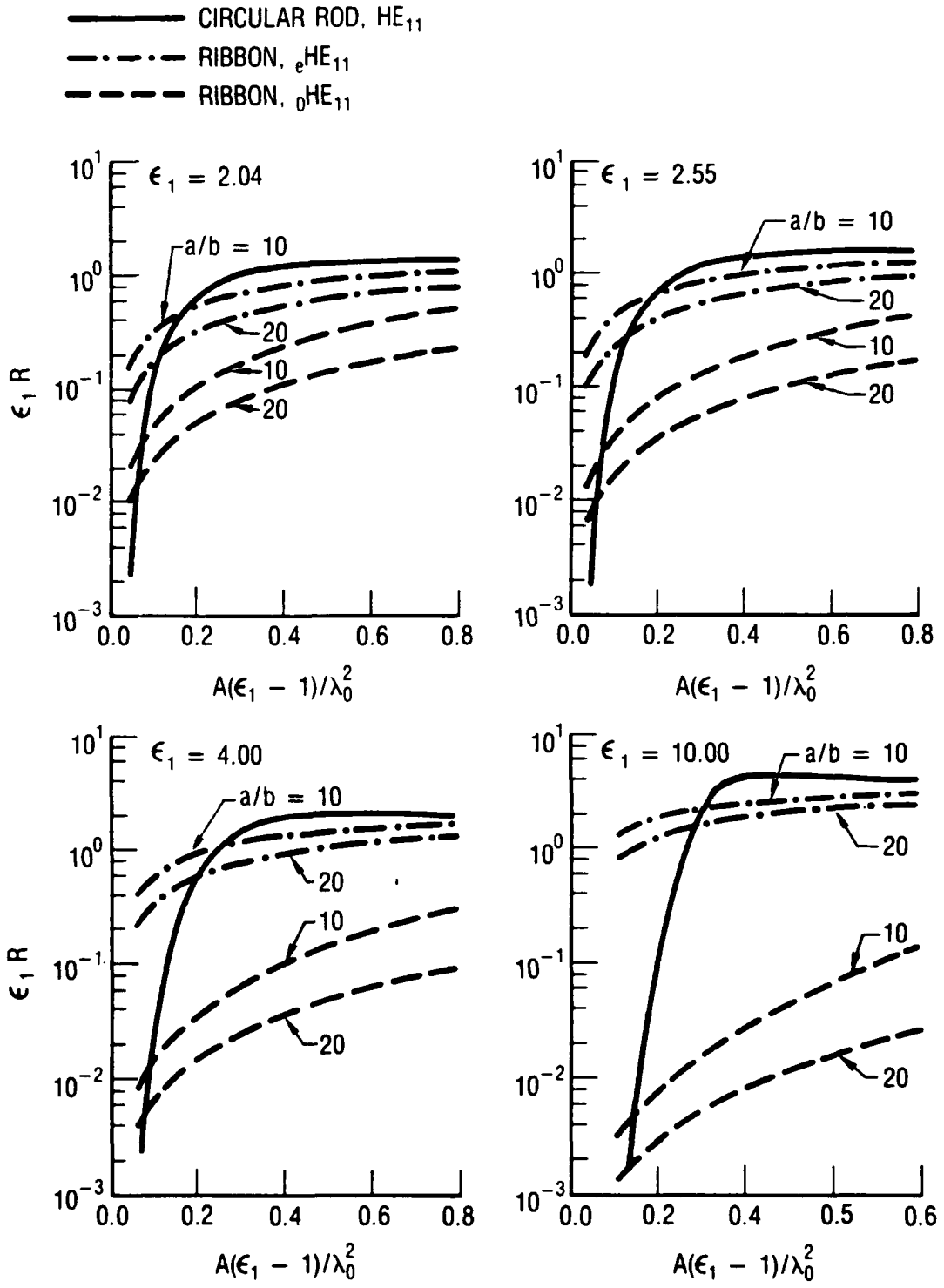

Fig. 6. Configuration Loss Factor $\epsilon_1 R$ as a Function of Normalized Frequency for a Dielectric Ribbon with Width 2a and Thickness 2b for Various Dielectric Material. This calculation is based on the slab approximation for which all fields, external as well as internal, are confined within a width of 2a. Note, for a given normalized frequency, the dramatic difference between the configuration loss factor for a ribbon supporting the low-loss TM wave and that for a circular rod supporting the HE_{11} mode, especially for higher dielectric constant material.

The advantage of ribbon guide over circular rod guide is also shown in Fig. 7, where the loss-factor ratio, $\varepsilon_1 R$ (for circular rod)/$\varepsilon_1 R$ (for ribbon), is plotted against the normalized cross-sectional area. Again the dramatic difference is seen between the ribbon guide and the circular rod guide. For example, with $\varepsilon_1 = 10$ (sapphire), if the normalized area is 0.35, the ratio could be as high as 400 for a ribbon with aspect ratio of 20:1, indicating that the loss factor for a ribbon guide could be as much as 400 times less than that for a circular rod. These curves also indicate the advantage of using high-dielectric-constant and low-loss tangent material to construct ribbon waveguides. This advantage is demonstrated in Fig. 8.

A major concern of any open-guiding structure is the field extent outside the core region. The loss factor for a flat ribbon can be made so much smaller than that for an equivalent circular rod primarily because of the spreading of the guided power in the lossless outer (noncore) region. But the distinguishing feature of a ribbon guide is its expanding surface area, which enables the guided mode to attach to it. Conversely, the circular rod possesses minimal surface area; hence, its guided mode (in the low-loss region) tends to loosely attach to the guide and can easily detach itself and become a radiated wave. Figure 9 exhibits how rapidly the power density of the guided mode decays from the core surface of the four low-loss guiding materials. The normalized distance, d/λ_0, is plotted against the normalized area. In this figure, d is the distance from the core surface at which the power density of the guided mode has decayed to 1/e of its value at the core surface. For typical operating range ($0.2 \leq A(\varepsilon_1 - 1)/\lambda_0^2 \leq 1.0$), the normalized field extent, d/λ_0, is less than 0.5. In other words, it is safe to conclude that most of the guided power is confined within a region whose outer boundary is situated at least one free-space wavelength away from the core boundary. For mm or sub-mm operation, this requirement is easily accommodated.

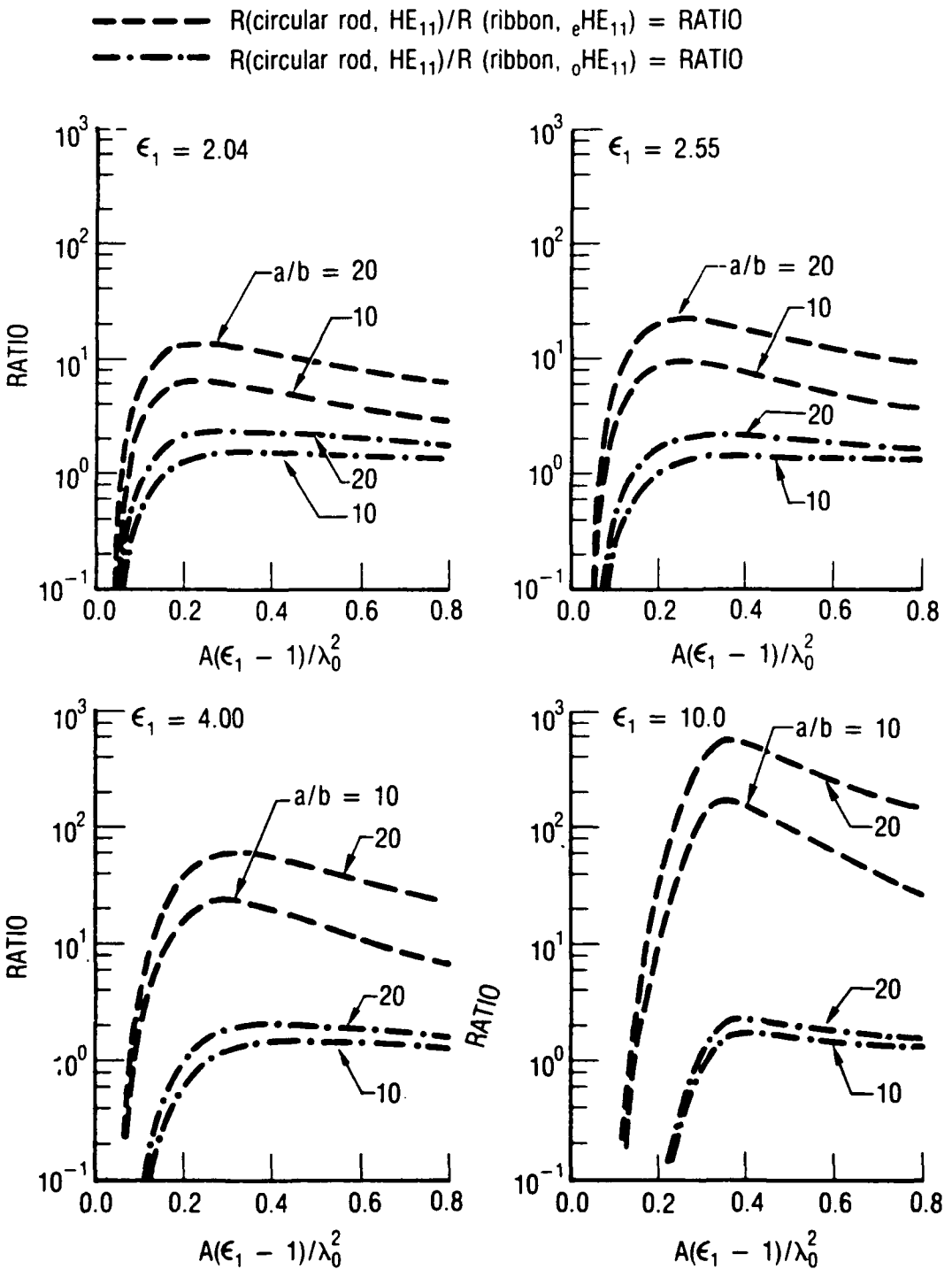

Fig. 7. Ratio of the Configuration Loss Factor for Circular Rod and Ribbon vs the Normalized Frequency for Ribbon of Various Aspect Ratios and for Different Dielectric Material. Note that for ϵ_1 = 10 and a/b = 20, the ratio at $A(\epsilon_1 - 1)/\lambda_0^2$ = 0.35 is as high as 600.

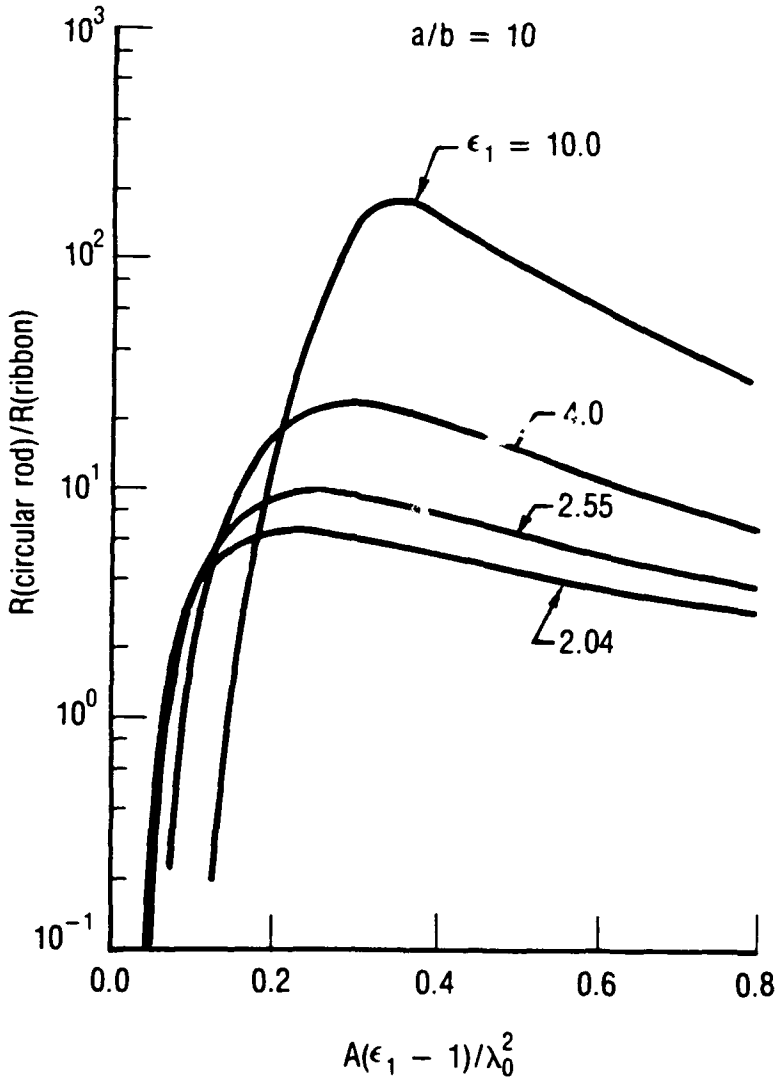

Fig. 8. Ratio of the Configuration Loss Factor for Circular Rod and Ribbon vs the Normalized Frequency for Ribbon with Aspect Ratio of 10 for Various Dielectric Material. Note the dramatic increase of the ratio as ϵ_1 is increased.

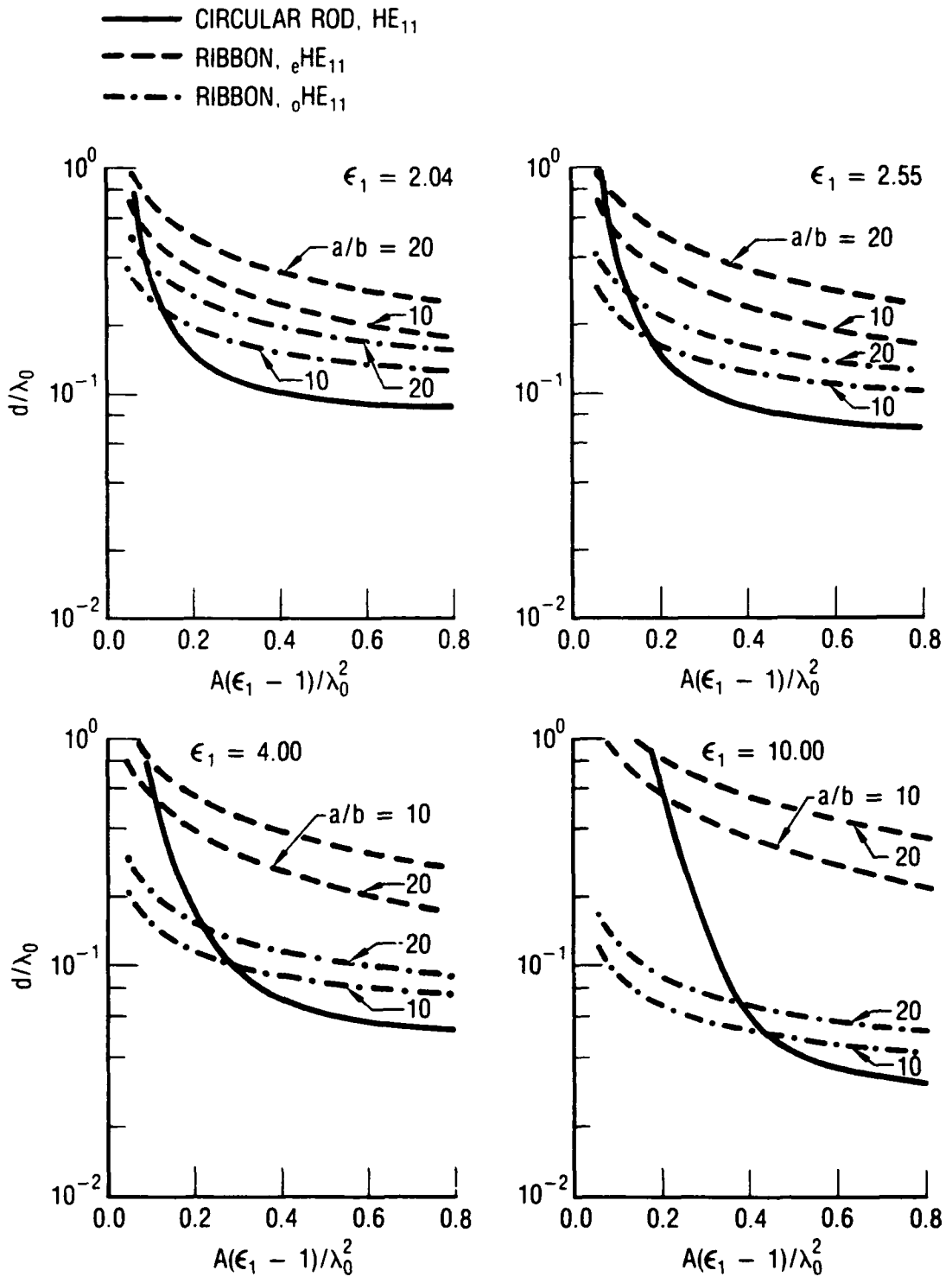

Fig. 9. Normalized Power-Decaying Distance d/λ_0 as a Function of Normalized Frequency for Various Ribbon Aspect Ratios and for Different Dielectric Material. d is the 1/e power-decaying distance from the surface of the ribbon or rod. Note that for all regions of interest (i.e., $0.2 < A(\epsilon_1 - 1)\lambda_0^2 < 0.8$), d is less than one free-space wavelength.

IV. THEORETICAL VERIFICATIONS

In the previous section, solution for a plane slab is used to form the solution for a ribbon with high aspect ratio. Further refinement of the slab solution can be obtained using an approximate approach developed by Marcatili.[6] In his formulation, the tangential fields are matched along the four sides of the rectangular core region, but the matching is ignored at the corners. The field components in the core region are assumed to vary sinusoidally in the two transverse directions along the major and minor axes. In the regions above and below the core, the fields vary sinusoidally along the direction of the major axis and decay exponentially along the direction of the minor axis away from the core. In the regions to the left and right of the core, the fields vary sinusoidally along the minor axis and decay exponentially along the major axis. Marcatili then obtained a dispersion relation from which the propagation constants of various modes could be calculated. For the low-loss TM wave, the propagation constant β can be found by solving the following equations:

$$2ak_x = \pi - 2\tan^{-1}\left[k_x/(k_1^2 - k_0^2 - k_x^2)^{1/2}\right]$$

$$2bk_y = \pi - 2\tan^{-1}\left[(k_y/\varepsilon_1)/(k_1^2 - k_0^2 - k_y^2)^{1/2}\right]$$

$$\beta^2 = k_1^2 - k_x^2 - k_y^2 \qquad (13)$$

where 2b and 2a are, respectively, the height and the width of the ribbon guide; $k_1^2 = \omega^2\mu\varepsilon_1\varepsilon$; and $k_0^2 = \omega^2\mu\varepsilon_0\varepsilon$. The configuration loss factor $R^{(TM)}_{Marcatili}$ is

$$R^{(TM)}_{Marcatili} = |I|/(\sqrt{\mu/\varepsilon}\,|I_p|) \qquad (14)$$

with

$$I = (\omega\varepsilon_1\beta)^{-2}\, ab\{(k_x k_y^2[1 - \text{sinc}\,(2k_x a)][1 - \text{sinc}\,(2k_y b)]$$

$$+ (k_1^2 - k_y^2)^2\,[1 + \text{sinc}\,(2k_x a)][1 + \text{sinc}\,(2k_y b)]$$

$$+ (\beta k_y)^2\,[1 + \text{sinc}\,(2k_x a)]\,[1 - \text{sinc}\,(2k_y b)]\}$$

$$I_p = (k_1^2 - k_y^2)ab(\omega\varepsilon_1\beta)^{-1}\,[1 + \text{sinc}\,(2k_x a)][1 + \text{sinc}\,(2k_y b)]$$

$$+ (k_1^2 - k_y^2)a(\omega\varepsilon_0\beta)^{-1}(k_1^2 - k_0^2 - k_y^2)^{-1/2}\,[1 + \text{sinc}\,(2k_x a)]\cos^2(k_y b)$$

$$+ (k_0^2 - k_y^2)b(\omega\varepsilon_0\beta)^{-1}(k_1^2 - k_0^2 - k_x^2)^{-1/2}\cos^2(k_x a)[1 + \text{sinc}\,(2k_y b)]$$

To compare the configuration loss factors, $R^{(TM)}_{\text{Marcatili}}$ with $R^{(TM)}$ (according to the slab model), we introduce Fig. 10. In this figure, the normalized configuration loss factors for Marcatili's model and the slab model are plotted against the normalized area. For normalized frequency larger than 0.1, and $b/a > 3$, the loss factors for both models are quite close to each other, indicating that the slab model approximation is close to Marcatili's approximation. Also, as aspect ratio increases for the rectangular dielectric waveguide, the loss factor based on Marcatili's approximation approaches that based on the slab model. Note that Marcatili's curves are above the slab model curves. This means that the nonuniform distribution of the electric field intensity within the rectangular core region tends to increase the configuration loss factor. This conclusion is consistent with our previous conjecture that achieving the uniform distribution of the electric field intensity within the core region promotes the low-loss behavior of the guided mode. Hence, flat ribbon with high aspect ratio appears to be the optimal configuration in achieving a low-loss factor.

The preceding results, shown in Fig. 10, re-affirm the validity of the slab model in providing a good theoretical guideline for designing ultralow-loss ribbon dielectric waveguides.

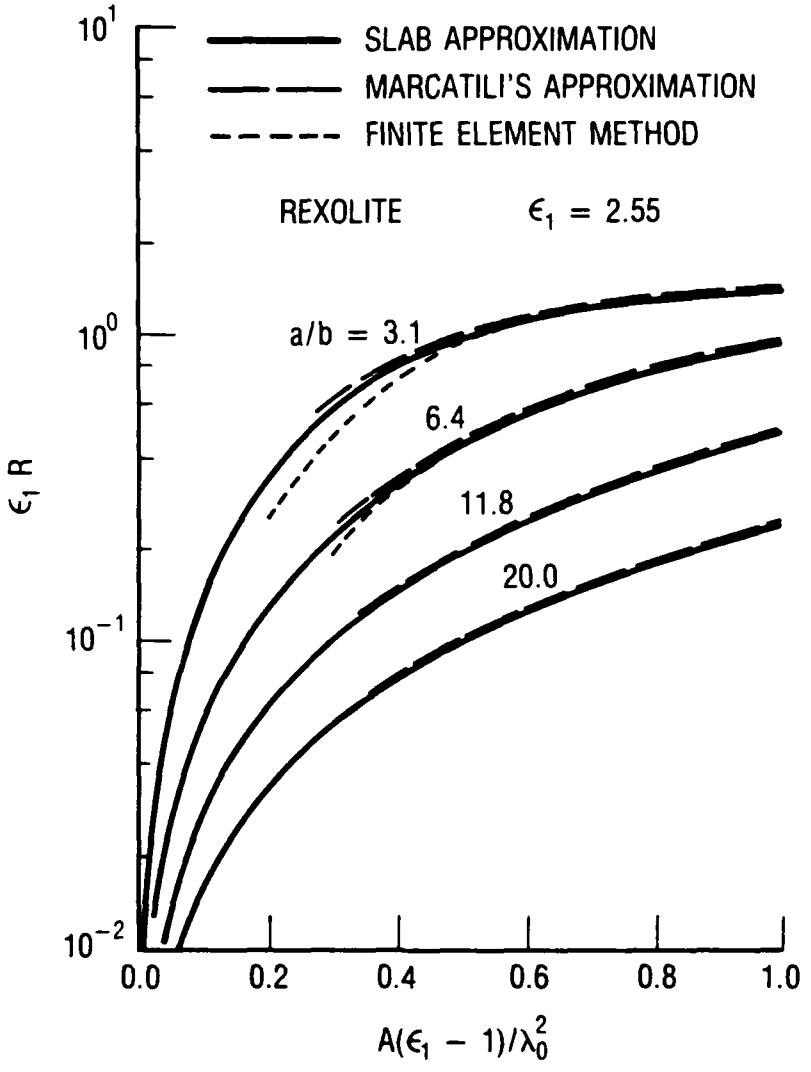

Fig. 10. Configuration Loss Factor vs Normalized Frequency for the Dielectric Ribbon Waveguide. Results are obtained according to two approximate methods, the slab approximation and Marcatili's approximation, and to one exact method, the finite element method. Within the region of interest, i.e., $0.3 < A(\epsilon_1 - 1)/\lambda_0^2 < 2.0$, results from approximate methods agree very closely with those from the exact method for flat ribbon with $a/b \geq 10$, where 2a is the width and 2b is the thickness of the ribbon; the differences are noticeable only when $a/b < 6.4$. This graph reveals that the approximation approaches can be used with confidence to predict the configuration loss factor behavior for thin ribbons.

For further validation of the slab model, an exact approach based on the solution of Maxwell's equations by the finite element approach is used to calculate the configuration loss factor. According to this finite element approach,[7] the governing longitudinal fields of the guided wave are first expressed as a functional, as follows:

$$I = \sum_{p=1} I_p$$

$$= \sum_{p=1} \iint \left(\tau_p |\nabla H_z^{(p)}|^2 + \gamma^2 \tau_p \, \varepsilon_p \left| \frac{1}{\gamma} \left(\frac{\varepsilon_0}{\mu} \right)^{1/2} \nabla E_z^{(p)} \right|^2 \right.$$

$$+ 2\gamma^2 \tau_p \hat{e}_z \cdot \left[\frac{1}{\gamma} \left(\frac{\varepsilon_0}{\mu} \right)^{1/2} \nabla E_z^{(p)} \times \nabla H_z^{(p)} \right]$$

$$\left. - \left(\frac{\omega}{c} \right)^2 (\gamma^2 - 1) \left\{ (H_z^{(p)})^2 + \gamma^2 \frac{\varepsilon_p}{\varepsilon_0} \left[\frac{1}{\gamma} \left(\frac{\varepsilon_0}{\mu} \right)^{1/2} E_z^{(p)} \right]^2 \right\} \right) \qquad (15)$$

where

$$\gamma = \frac{\beta c}{\omega}, \quad \tau_p = \frac{\gamma^2 - 1}{\gamma^2 - \varepsilon_p},$$

ε_p is the dielectric constant in the pth region, $\hat{e}_z$ is a unit vector in the z direction, and c is the speed of light in vacuum. The symbol p represents the pth region when one divides the guiding structure into many appropriate regions. Minimizing the preceding surface integral over the whole region is equivalent to satisfying the wave equation and the boundary conditions for E_z and H_z. In the finite element approximation, the primary dependent variables are replaced by a system of discretized variables over the domain of consideration. Therefore, the initial step is a discretization of the original domain into many subregions. For the present analysis, there are a number of regions in the composite cross section of the waveguide for which the permittivity is distinct. Each of these regions is discretized into a number of smaller triangular subregions interconnected at a finite number of

points, called nodes. Appropriate relationships can then be developed to represent the waveguide characteristics in all triangular subregions. These relationships are assembled into a system of algebraic equations governing the entire cross section. Taking the variation of these equations with respect to the nodal variable leads to an algebraic eigenvalue problem, from which the propagation constant for a certain mode may be determined. The longitudinal electric field, $E_z^{(p)}$, and the longitudinal magnetic field, $H_z^{(p)}$, in each subdivided pth region are also generated in this formalism. All transverse fields in the pth region can be produced subsequently from the longitudinal fields. Complete knowledge of the fields can be used to generate the configuration loss factor according to Eq. (4). Results are also shown in Fig. 10, in which the configuration loss factors for four rectangular ribbon guides with aspect ratios of 3.1, 6.4, 11.8, and 20, are plotted as a function of their normalized areas. In the same figure, results based on the slab model, as well as on Marcatili's approximation, are also given. As shown, when the aspect ratio is 3.1, the curve based on the exact analysis is substantially below the curves based on Marcatili's method or on the slab model. As expected, however, the agreement is better for higher frequencies and for higher aspect ratio rectangular guides. In fact, one may conclude from Fig. 10 that, for the ribbon guide with large aspect ratios [(height/width) $>$ 5], and for the frequency region [area$(\varepsilon_1 - 1)$/(free-space wavelength)^2] $>$ 0.3, the configuration loss factor calculated according to Marcatili's method or the slab model gives an extremely good approximation to the true value.

V. EXPERIMENTAL VERIFICATIONS

The exceptionally low-loss behavior of the dielectric ribbon waveguide supporting the dominant $_eHE_{11}$ mode will now be verified by measurements. A newly designed dielectric waveguide cavity resonator that is capable of supporting the dominant mode is used.[8] A schematic diagram of the measurement setup is shown in Fig. 11.

A dielectric rod resonant cavity consists of a dielectric waveguide of length d terminated at its ends by sufficiently large, flat, and highly reflecting plates that are perdendicular to the axis of the guide. Microwave energy is coupled into and out of the resonator through small coupling holes at both ends of the cavity. For best results, the holes are dimensioned so that they are beyond cutoff. At resonance, the length of the cavity, d, must be $m\lambda_g/2$ (m is an integer), where λ_g is the guide wavelength of the particular mode under consideration. By measuring the resonant frequency of the cavity, one may obtain the guide wavelength of that particular guided mode in the dielectric waveguide. The propagation constant, β, of that mode is related to λ_g and v_p, the phase velocity, as follows:

$$\beta = \frac{2\pi}{\lambda_g} = \frac{\omega}{v_p} \tag{16}$$

The Q of a resonator is indicative of the energy storage capability of a structure relative to the associated energy dissipation arising from various loss mechanisms, such as those resulting from the imperfection of the dielectric material and the finite conductivity of the end plates. The common definition for Q is applicable to the dielectric rod resonator and is given by

$$Q = \omega \frac{\bar{W}}{\bar{P}} \tag{17}$$

where ω is the angular frequency of oscillation, $\bar{W}$ is the total time-averaged energy stored, and $\bar{P}$ is the average power loss. Three rexolite dielectric strip waveguides were fabricated and placed in a parallel plate resonator. The dimensions of these waveguides are listed in Table 2.

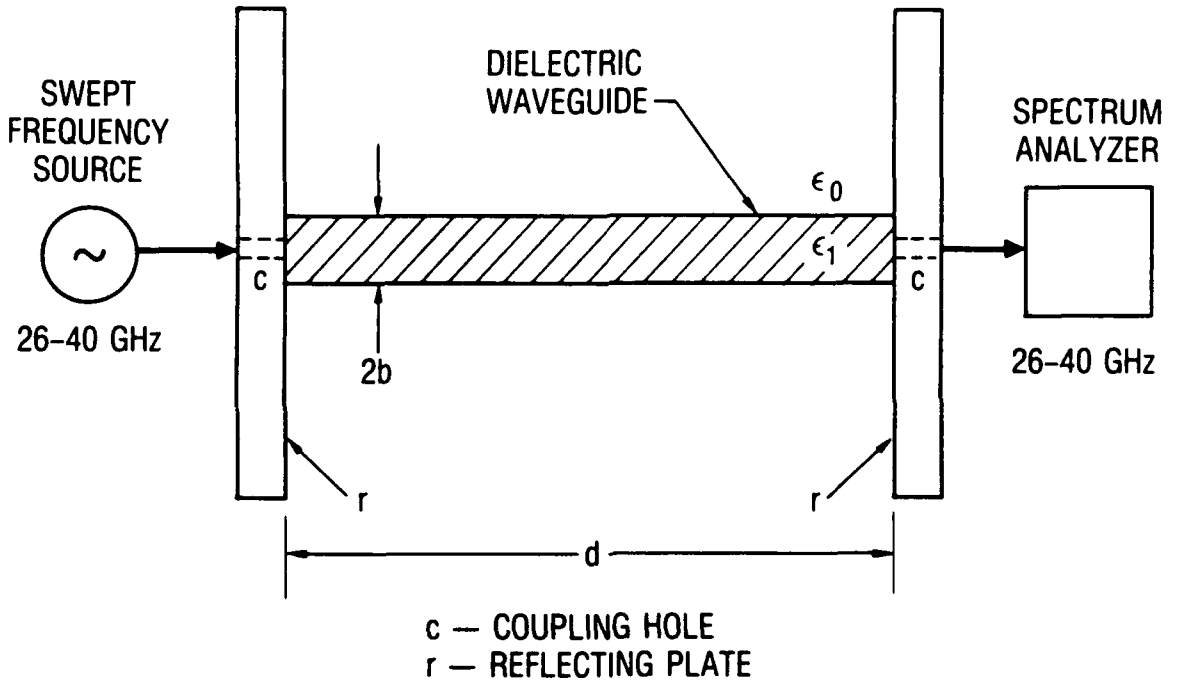

Fig. 11. Schematic Diagram of the Experimental Setup

Table 2. Rexolite Strip Waveguides

$\varepsilon_1 = 2.55$

$\tan\delta = 0.9 \times 10^{-3}$

	2a, cm	2b, cm	a/b	L, cm	Area, cm^2
Waveguide 1	0.767	0.251	3.1	20.32	0.193
Waveguide 2	1.072	0.167	6.4	20.32	0.180
Waveguide 3	1.40	0.14	10	60.96	0.195

The measurement procedure was described in a previous paper.[8] The coupling was such that only the dominant mode was excited, and the primary loss mechanism in the resonator was the dielectric loss. A swept signal was coupled into the cavity; the output was a series of narrow resonances. The resonant frequencies and half-power bandwidths were measured with the spectrum analyzer. At each resonance, the Q was given by

$$Q_m = \frac{f_m}{\Delta f_m} \tag{18}$$

where f_m is the mth resonance and Δf_m is the half-power bandwidth at that resonance. Plots of the measured Q's for these waveguides are shown in Fig. 12. As explained in reference 8, the primary loss mechanism in this measurement configuration is the dielectric loss, and the measurement Q is the dielectric Q. For this case, the relation between α and Q is[8,12]

$$\alpha = (v_p/v_g)\beta/(2Q) \tag{19}$$

and the measured $\varepsilon_1 R$ is given by

$$\varepsilon_1 R = (v_p/v_g)(\beta/Q)/(\omega\sqrt{\mu\varepsilon_0}\,\tan\delta) \tag{20}$$

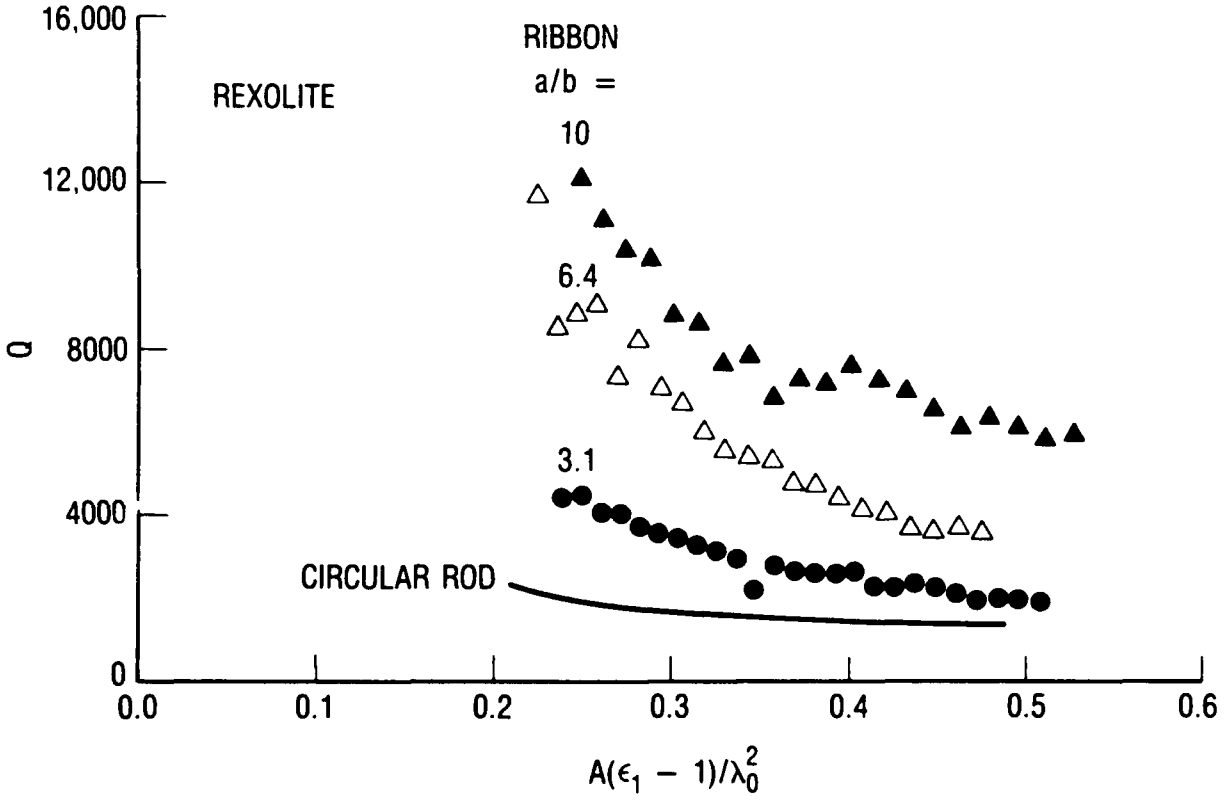

Fig. 12. Measured Q as a Function of Frequency for the Four Rexolite Waveguides. The dielectric constant and loss tangent of rexolite are, respectively, 2.55 and 0.9×10^{-3}. Only the low-loss $_eHE_{11}$ mode is supported by the structure.

where β, v_p, and v_g were measured as described in reference 8, and $\tan\delta$ is the value previously determined for rexolite. Figure 13 exhibits a plot of the external power density distribution across the three waveguides using an electric probe. The height of the probe was positioned so that the power level was 10 dB below the level at the surface of the waveguide. At this level, the Q was not significantly affected by the presence of the probe. Figure 14 exhibits plots of the external power density decay away from the surface of the waveguide, along with the calculated values. Figure 15 displays plots of the measured $\varepsilon_1 R$'s for the rexolite rectangular waveguides, along with the calculated values for these waveguide dimensions. Excellent agreement was found for all three samples used in our experiment.

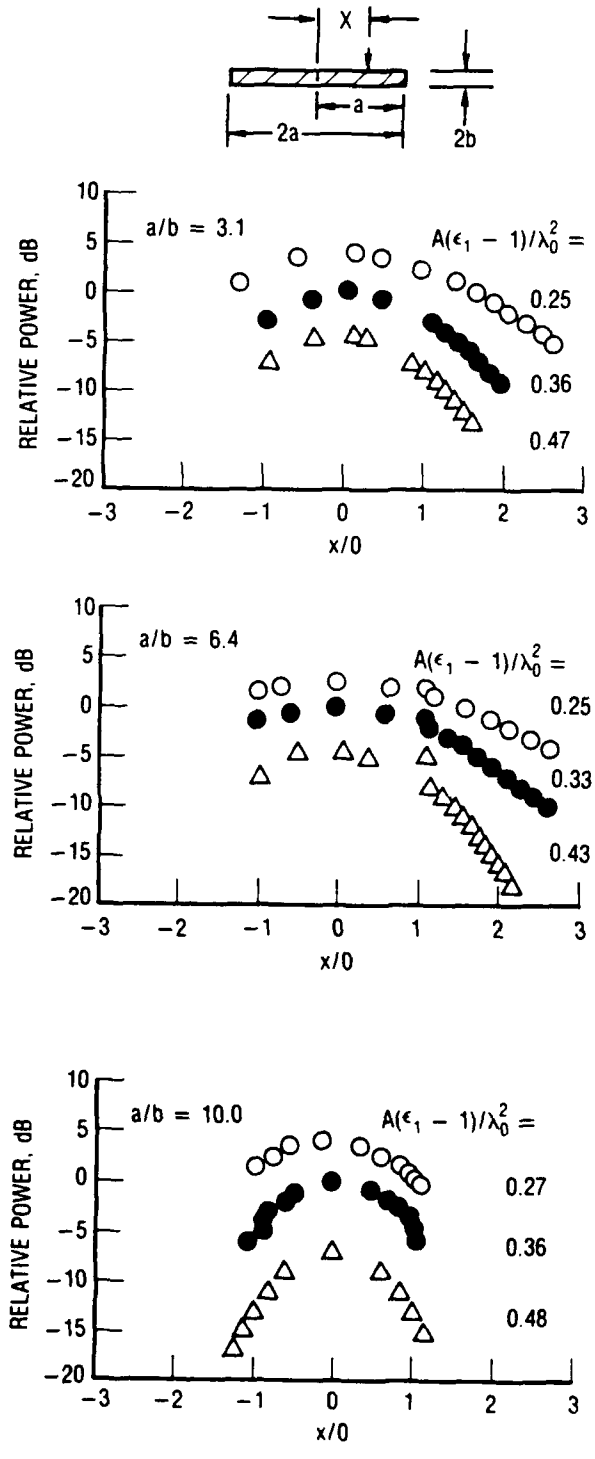

Fig. 13. External Power Density Distribution for the Guided Mode for Three Rexolite Waveguide Samples

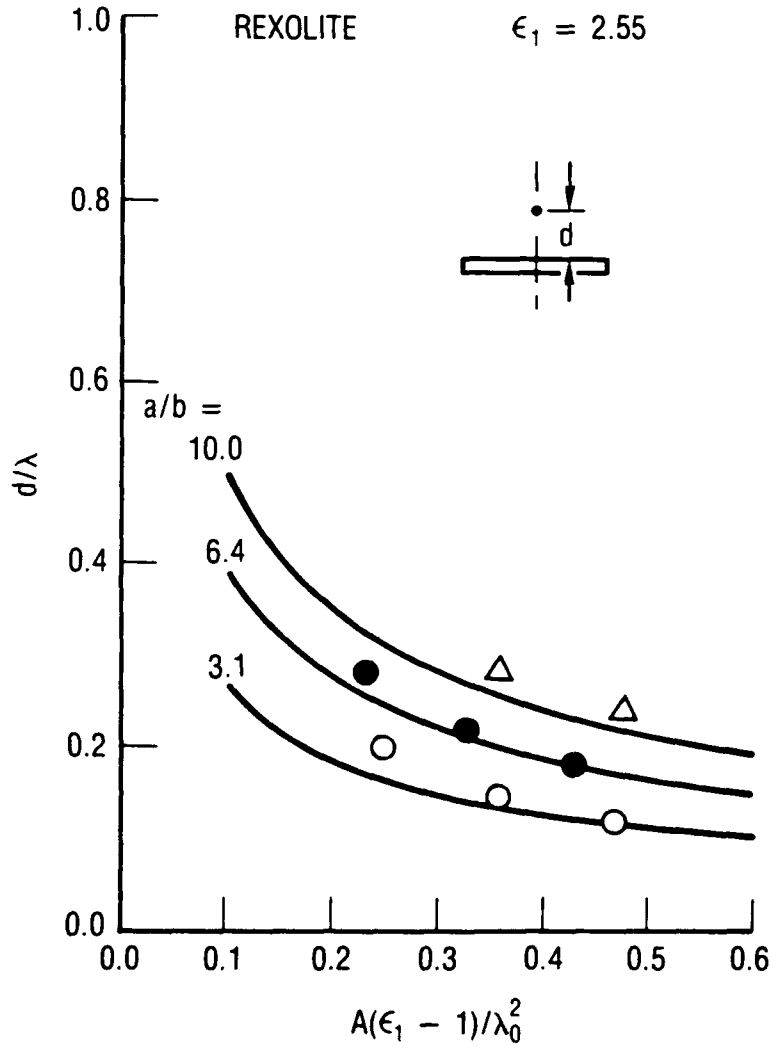

Fig. 14. External Power Density as a Function of the Normalized Distance d/λ_0, where d is the Distance Away from the Surface of the Guide. Solid lines are calculated results.

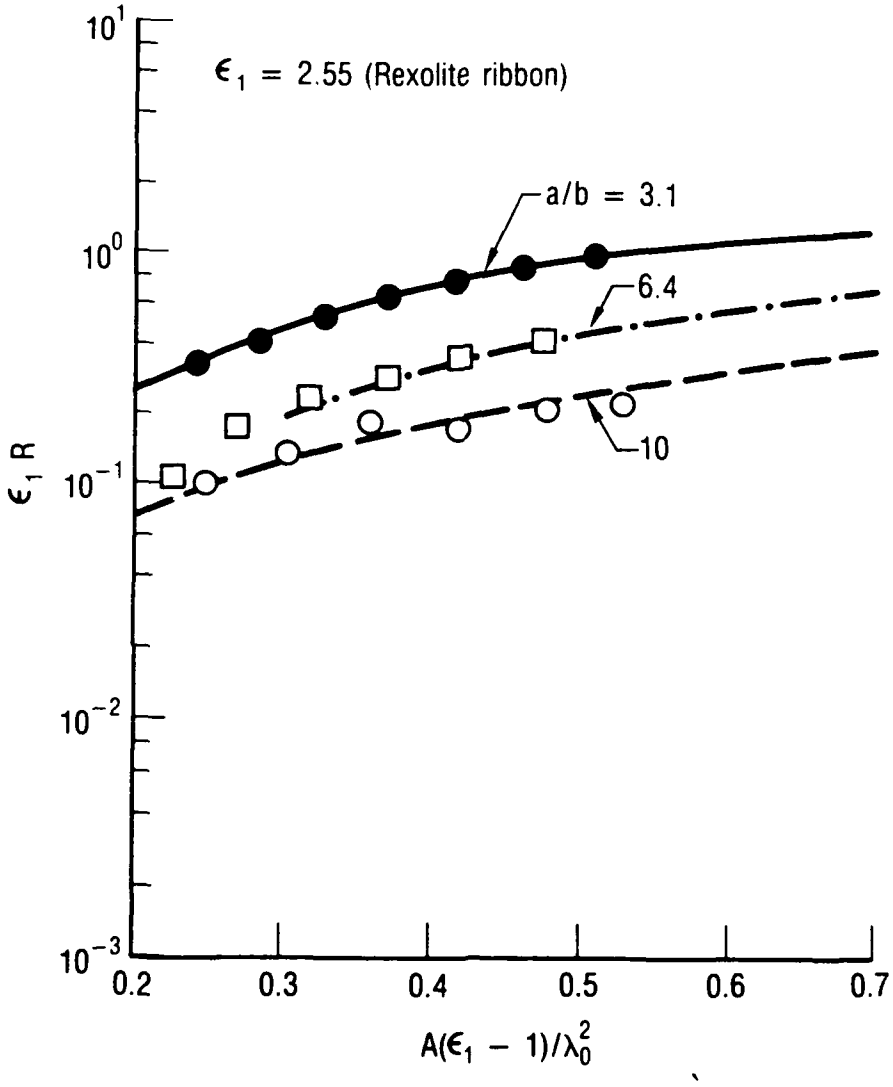

Fig. 15. Comparison Between Calculated Configuration Loss Factor with Measured Data for Dielectric Ribbon Waveguide with Three Different Aspect Ratios. Points are experimental data; curves are theoretical results.

VI. CONCLUSIONS

This investigation shows that, by using a high-apsect ratio ($a/b > 10$), dielectric-ribbon waveguide made with high-dielectric constant ($\epsilon_1 > 9$) and low-loss ($\tan\delta_1 \approx 10^{-4}$) material, an ultralow-loss mm/sub-mm wave transmission system can be designed with the following features.

1. Extremely low attenuation constant for the dominant guided mode. The attenuation constant can be made lower than 10 to 20 dB/km in the mm/sub-mm wavelength range.

2. Known low-loss dielectric material such as alumina, quartz, or sapphire. No major breakthrough in the search of low-loss material is needed to achieve the target of less than 10 to 20 dB/km attenuation constant.

3. Flexible guide, i.e., the guide can turn corners.

4. Economical and easy-to-manufacture guide.

5. Electromagnetic pulse (EMP)-resistant guide.

6. Guide that presents relatively low scattering profile, unlike metallic structure.

7. Ease in coupling power into and out of the guiding structure.

8. Photolithographic techniques, which enable circuits to be conveniently etched on waveguide surface.

Realization of our ultralow-loss dielectric waveguide will encourage further development in the perfection of a new class of low-loss dielectric waveguides and components for use in the mm/sub-mm wavelength range.

REFERENCES

1. M. N. Afsar and K. J. Button, "Millimeter-Wave Dielectric Measurement of Materials," Proc. IEEE 73, 131-153 (1985); R. Birch, J. D. Dromey, and J. Lisurf, "The Optical Constants of Some Common Low-Loss Polymers Between 4 and 40 cm^{-1}," Infrared Physics 21, 225-228 (1981).

2. M. N. Afsar, "Precision Dielectric Measurements of Nonpolar Polymers in the Millimeter Wavelength Range," IEEE Trans. on Microwave Theory and Tech. MTT-33, 1410-1415 (1985).

3. J. R. Birch and T. J. Parker, Infrared and Millimeter Wave, Vol. 2, ed. K. J. Button, Academic Press, New York (1979).

4. William B. Bridges, "Low Loss Flexible Dielectric Waveguide for Millimeter Wave Transmission and Its Application to Devices," Report Nos. SRO-005-1 and SRO-005-2 California Institute of Technology, Pasadena (1979-1982); William B. Bridges, Marvin B. Kline, and Edgard Schweig, IEEE Trans. on Microwave Theory and Tech. MTT-30, 286-292 (1982).

5. S. Ramo, J. R. Whinnery, and T. VanDuzer, Fields and Waves in Communication Electronics, Second Ed., John Wiley & Sons, New York (1984).

6. E. A. J. Marcatili, Bell Sys. Tech. J. 48, 2071 (1969).

7. C. Yeh, K. Ha, S. B. Dong, and W. P. Brown, "Single-Mode Optical Waveguides," Appl. Opt. 18, 1490-1504 (1979).

8. F. I. Shimabukuro and C. Yeh, "Attenuation Measurement of Very Low Loss Dielectric Waveguides by the Cavity Resonator Method Applicable to Millimeter/Submillimeter Wavelength Range," IEEE Trans. on Microwave Theory and Techniques MTT-36, 1160-1167 (1988).

9. C. Yeh, "Attenuation in a Dielectric Elliptical Cylinder," IEEE Trans. on Antennas and Propagation AP-11, 177-184 (1963).

10. R. E. Collin, Field Theory of Guided Waves, McGraw-Hill Book Co., New York, NY (1960).

11. C. Yeh, "On Single-Mode Polarization Preserving Multi-Layered Optical Fiber," J. Electromagnetic Waves and Applications 2, 379-390 (1988).

12. C. Yeh, "A Relation Between α and Q," Proc. IRE 50, 2143 (1962).

LABORATORY OPERATIONS

The Aerospace Corporation functions as an "architect-engineer" for national security projects, specializing in advanced military space systems. Providing research support, the corporation's Laboratory Operations conducts experimental and theoretical investigations that focus on the application of scientific and technical advances to such systems. Vital to the success of these investigations is the technical staff's wide-ranging expertise and its ability to stay current with new developments. This expertise is enhanced by a research program aimed at dealing with the many problems associated with rapidly evolving space systems. Contributing their capabilities to the research effort are these individual laboratories:

Aerophysics Laboratory: Launch vehicle and reentry fluid mechanics, heat transfer and flight dynamics; chemical and electric propulsion, propellant chemistry, chemical dynamics, environmental chemistry, trace detection; spacecraft structural mechanics, contamination, thermal and structural control; high temperature thermomechanics, gas kinetics and radiation; cw and pulsed chemical and excimer laser development, including chemical kinetics, spectroscopy, optical resonators, beam control, atmospheric propagation, laser effects and countermeasures.

Chemistry and Physics Laboratory: Atmospheric chemical reactions, atmospheric optics, light scattering, state-specific chemical reactions and radiative signatures of missile plumes, sensor out-of-field-of-view rejection, applied laser spectroscopy, laser chemistry, laser optoelectronics, solar cell physics, battery electrochemistry, space vacuum and radiation effects on materials, lubrication and surface phenomena, thermionic emission, photosensitive materials and detectors, atomic frequency standards, and environmental chemistry.

Electronics Research Laboratory: Microelectronics, solid-state device physics, compound semiconductors, radiation hardening; electro-optics, quantum electronics, solid-state lasers, optical propagation and communications; microwave semiconductor devices, microwave/millimeter wave measurements, diagnostics and radiometry, microwave/millimeter wave thermionic devices; atomic time and frequency standards; antennas, rf systems, electromagnetic propagation phenomena, space communication systems.

Materials Sciences Laboratory: Development of new materials: metals, alloys, ceramics, polymers and their composites, and new forms of carbon; nondestructive evaluation, component failure analysis and reliability; fracture mechanics and stress corrosion; analysis and evaluation of materials at cryogenic and elevated temperatures as well as in space and enemy-induced environments.

Space Sciences Laboratory: Magnetospheric, auroral and cosmic ray physics, wave-particle interactions, magnetospheric plasma waves; atmospheric and ionospheric physics, density and composition of the upper atmosphere, remote sensing using atmospheric radiation; solar physics, infrared astronomy, infrared signature analysis; effects of solar activity, magnetic storms and nuclear explosions on the earth's atmosphere, ionosphere and magnetosphere; effects of electromagnetic and particulate radiations on space systems; space instrumentation.